Status of the Korba groundwater resources (Tunisia): observations and three-dimensional modelling of seawater intrusion

Jaouher Kerrou · Philippe Renard · Jamila Tarhouni

Abstract The Korba aquifer is located in the east of the Cape Bon peninsula in Tunisia. A large groundwater depression has been created in the central part of the aquifer since the 1980s, due to intense groundwater pumping for irrigation. The data collected show that the situation continues to deteriorate. Consequently, seawater is continuing to invade a large part of the aquifer. To better understand the situation and try to forecast its evolution, a three-dimensional (3D) transient density-dependent groundwater model has been developed. The model building process was difficult because of data required on groundwater discharge from thousands of unmonitored private wells. To circumvent that difficulty, indirect exhaustive information including remote sensing data and the physical parameters of the aquifer have been used in a multi-linear regression framework. The resulting 3D model shows that the aquifer is over-exploited. It also shows that after 50 years of exploitation, the time needed to turn back to the natural situation would be about 150 years if the authorities would ban all exploitation now. Such an asymmetry in the time scales required to contaminate or remediate an aquifer is an important characteristic of coastal aquifers that must be taken into account in their management.

Keywords Seawater intrusion · Numerical modelling · Remote sensing · Multivariate statistics · Tunisia

Received: 31 May 2009 / Accepted: 5 January 2010
Published online: 25 March 2010

J. Kerrou (✉) · P. Renard
Centre for Hydrogeology,
University of Neuchâtel,
Rue Emile Argand, 11-CP158, 2009, Neuchâtel, Switzerland
e-mail: jaouher.kerrou@unine.ch
Tel.: +41-32-7182602
Fax: +41-32-7182603

J. Tarhouni
Institut National Agronomique de Tunisie,
Avenue Charles Nicolle, 43, 1082, Tunis-Mahrajène, Tunisia

Introduction

The Korba coastal plain is located in the east of the Cape Bon peninsula in north-eastern Tunisia (Fig. 1). It encompasses an area of around 40 km × 10 km, bounded by the Mediterranean Sea along the eastern border. The area is characterized by a semiarid climate with an average annual precipitation of 420 mm (INM 2001), which is significantly higher than in the rest of Tunisia, where the average annual precipitation is around 220 mm (INM 2001). This is one of the reasons why the Cape Bon was always one of the most productive agricultural areas in Tunisia. The agricultural activity, together with the population growth in the country—from 3.78 million inhabitants in 1956 to 9.91 million in 2004 (INS 2004)—and the developing economy, have greatly increased the freshwater demand. Consequently, and since the 1960s, groundwater has become a major resource in the Cape Bon area and has been solicited mainly for agricultural purposes. The exploitation of the Korba aquifer has increased almost linearly from 270 wells pumping 4 Mm^3 (million m^3) in 1962 (Ennabli 1980) to more than 8,000 wells pumping 50 Mm^3 in 1985 (DGRE 1985). This increase resulted in a regional depletion of the water table and salinization caused by seawater intrusion (Tarhouni et al. 1996).

Even if these problems are common to a large number of coastal aquifers worldwide (Bear et al. 1999; Custodio 2002; Cheng and Ouazar 2003; Konikow and Kendy 2005), the depletion of the water table in the Korba aquifer was first observed in the early 1970s, and the salinization by seawater intrusion was not recognized as a serious threat until the mid 1980s. Since then, the situation has motivated numerous studies on the Korba aquifer.

Ennabli (1980) presented a detailed description of the regional geology and the main aquifers as well as the state of the groundwater resources in 1977. With the existing data at that time, Ennabli developed a first conceptual model of the aquifer system. A two-dimensional (2D) numerical model showed an estimation of the areal recharge in the range of 5–8% of the average annual precipitation (21–34 mm), a transmissivity ranging from 5×10^{-5} to 10^{-2} m^2/s and an average porosity of 0.12 (Ennabli 1980). This value, together with an estimated seasonal head variation of 0.88 m (Ennabli 1980), allowed a first estimation of the groundwater regulatory reserve.

 DOI 10.1007/s10040-010-0573-5

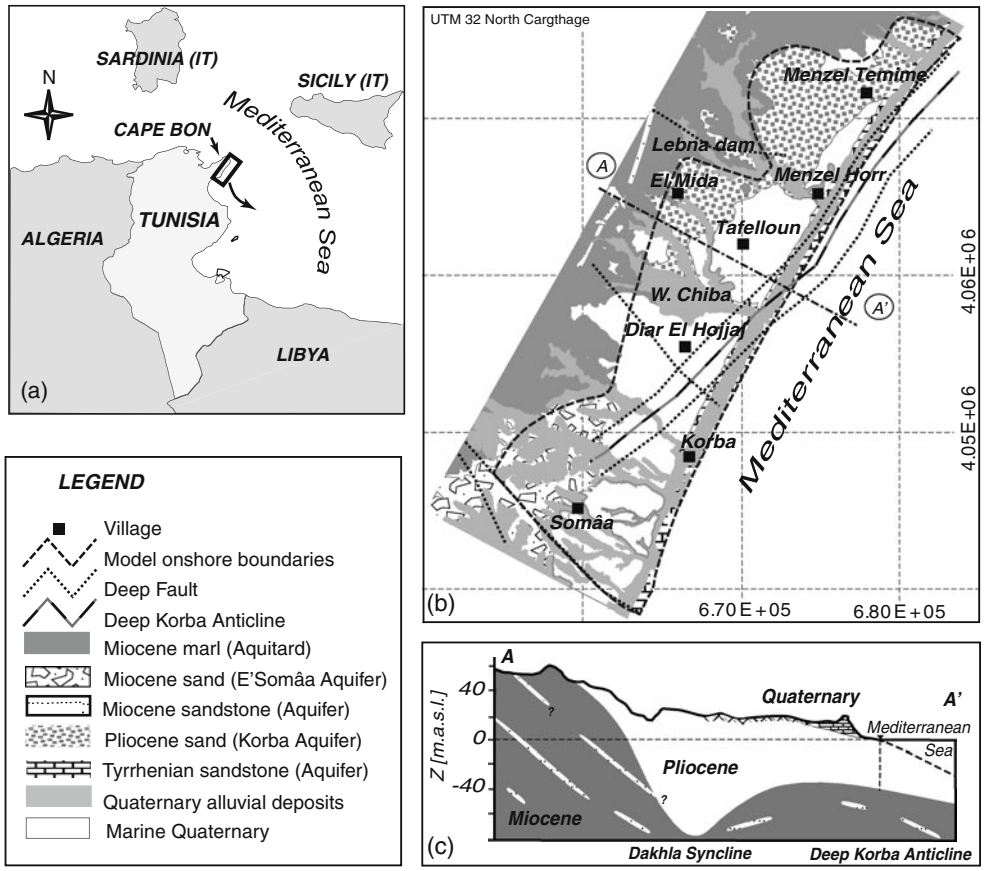

Fig. 1 **a** Location of the Korba aquifer, **b** geological setting (square size is 10×10 km), **c** simplified cross-section. Note: the *question marks* mean that the extension of those units is not well known; *Z* stands for elevation

Tarhouni et al. (1996) used a geochemical approach to determine the origin of aquifer salinization and showed that seawater intrusion is the main source of salt pollution. Khlaifi (1998) described the state of the resource in 1996 and showed that there is a piezometric depression of 5 m below the mean sea level around Diar El Hojjaj in the central part of the aquifer (Fig. 1) and the salinization of wells up to 1.5 km inland (up to 7 g/l). This resulted in the abandonment of hundreds of wells close to the sea. Paniconi et al. (2001) elaborated a three-dimensional (3D) numerical model of the status of the Korba aquifer in the late 1990s. The authors showed the ability of the CODESA-3D code (Gambolati et al. 1999) to handle regional-scale seawater intrusion settings and the validity of using numerical models to investigate different groundwater management scenarios. However, the scenarios investigated by Paniconi et al. (2001) did not match expected groundwater mass balance, especially with regard to pumping rates.

In addition to a lack of sufficient data describing the hydraulic properties of the Korba aquifer, a particular difficulty is the large uncertainty concerning the pumping rates of thousands of private wells in the region. In 2000, the local water management authorities recorded more than 9,000 wells pumping altogether around 50 Mm^3/year (DGRE 2000). Most of these wells are located in very small private farms and are traditionally dug and equipped with motor pumps. None of those wells are equipped with a flowmeter and no survey has ever been made to exhaustively estimate the pumping rates. To make things worse, the local authorities use an administrative delimitation of the regional aquifers which does not correspond to their physical extent. Indeed, a good knowledge of the withdrawn volumes of groundwater is crucial in understanding the dynamics of the aquifer to further model seawater intrusion and to address optimal management scenarios.

Today, one of the major issues in the Korba plain, is to estimate how much groundwater can be exploited in a sustainable way, thus preventing seawater intrusion. Despite the governmental efforts to develop alternative sources of freshwater (construction of dams, water bypasses from the north of the country, distribution of efficient irrigation systems, reuse of treated waste water and artificial recharge of the aquifer), farmers still need to exploit the groundwater resources. As a first step in order to define sustainable exploitation rates, this paper describes a quantitative study of seawater intrusion in the Korba coastal aquifer. The main objectives of this work are: (1) to describe the recent state of the regional groundwater system by analyzing existing and newly collected data; (2) to apply different methods to better estimate the freshwater mass balance components, with a special focus on the abstraction volumes; (3) to use this

 DOI 10.1007/s10040-010-0573-5

information to elaborate a new transient 3D density-dependent flow and transport model to better understand the aquifer dynamics. In particular, the model is used to estimate in how much time the system could come back to its natural state.

This paper is organized as follows. Existing knowledge of the Korba aquifer is presented in section The Korba aquifer system. The 3D numerical model development is described in section The Korba aquifer numerical model development. Sections Simulations results and Discussion and conclusions present and discuss respectively the results of the simulations of groundwater mass balance and head and salt concentrations distributions. The paper ends with a set of conclusions and recommendations with regard to the management of the regional groundwater resources.

The Korba aquifer system

The data sets used in this study were provided mainly by the Institut National Agronomique de Tunisie (INAT) and the local groundwater management authority (CRDA Nabeul). Data were compiled in a geographic information system (GIS). Data sets include: rainfall, potential evapotranspiration, soil distribution map, land cover maps from 1996, geographical information (ephemeral streams, salt lakes, etc.), geological logs, transmissivity values estimated from pumping tests, piezometric levels, and total dissolved solids (TDS) measurements. In order to complete the data set and describe the recent state of the Korba aquifer, additional field investigations were carried out in August 2004. These include well leveling, water-table depth measurements and vertical salinity logs at selected wells.

Geological setting

The inland lateral extension of the Korba aquifer follows the outcropping geological boundaries (Fig. 1). The geology of the Cape Bon peninsula and its structural evolution is described by Ennabli (1980) and Bensalem (1992, 1995). Three main geological units of marine Quaternary, Pliocene and late Miocene ages constitute the Korba aquifer system (Fig. 1b). The Tyrrhenian Quaternary forms a 1.2 km-wide strip parallel to the coastline all along the study area (Fig. 1b, c). It is made of arenitic limestones overlying conglomeratic units (Oueslati 1994) with a total thickness ranging between 10 to 50 m.

The second unit, which represents the main aquifer, was formed during the Pliocene by marine deposits in the Dakhla synclinal north of Korba city (Fig 1c). The Dakhla syncline was formed during the Atlasic folding phase. It presents a north-east to south-west axis and is bounded by the Djebel Sidi Abderrahmane (639 m) anticline to the west and by the deep Korba anticline to the east (Fig. 1b,c). The lithology of the Pliocene formation is dominantly yellow sand with clay and sandstone intercalations. Laterally, the facies changes southward to more differentiated clay, sand and sandstone layers. The thickness of the Pliocene formation is about 80 m in the central part of the area, reaches 250 m offshore, decreasing towards the west (Fig. 1b). Note, however, that the thickness of the Pliocene sands in the north of Korba city is still unknown. Yet, it is believed to be relatively thin. Since the regression of the Pliocene sea, during the Quaternary and until today, the central part of the area was filled with alluvial material (Fig. 1b) deposited by *wadi* Chiba (*wadi*: dry stream except during periods of rainfall) and its effluents (Ennabli 1980).

The third unit, called "the Somâa sands", is of late Miocene age and found only to the south of the study area (Bensalem 1998). This unit is mainly composed by thick fine sand layers of continental origin including conglomeratic levels and clay lenses. To the south of the area, the thickness of the Somâa formation might exceed 400 m. Data from offshore oil wells allowed a better characterization of the aquifer system bellow the Mediterranean Sea. These data showed that the Pliocene and Somâa formations extend 2–5 km offshore where they thicken.

The geological aquifer units overly (with an angular discordance) mid-Miocene marls which form the base of the system (Fig. 1c). This aquitard may contain lenticular sandstone and clay-sandstone bars of variable thickness and depth but often separated by thick layers of impervious marls for a total thickness of 1,200 m (Abbes and Polak 1981).

Regional hydrogeology

The Korba aquifer can be divided into two hydrogeological units: the Plio-Quaternary and the late Miocene units. Northern and southern aquifer limits were delineated from flow streamlines almost perpendicular to the sea (Fig. 2b,d). A south-east to north-west oriented deep fault (Fig. 1b) helps to delineate the contour of the southern limit. Marine and continental deposits are laterally connected; the late Miocene aquifer feeds the Pliocene unit upstream. Yet, their hydraulic properties are significantly different. The Plio-Quaternary unit is the most productive one. It is characterized by the highest hydraulic conductivities, ranging from 10^{-6} to 10^{-3} m/s while hydraulic conductivities at the Somâa formation are smaller (Ennabli 1980). More precisely, the Tyrrhenian sandstones are believed to form the most permeable unit, followed by the central part of the Pliocene (alluvial deposits), the Pliocene, the Somâa and, finally, the early Miocene formations. These differences can be observed on the hydraulic gradients (Fig. 2) which range from 0.007 in the north to 0.014 in the south (in summer 2004). Ennabli (1980) proposed an average porosity of 0.12 for the whole aquifer system.

The Plio-Quaternary unit represents a typical unconfined coastal aquifer structure especially when it is outcropping (Fig. 1b) but might also be locally semi-confined due to less permeable lenses of large lateral extent. The Somâa unit in the southern part of the system is unconfined in the upstream area but confined close to the coastline where artesian wells existed until the mid 1990s. Another difference between the northern and the

 DOI 10.1007/s10040-010-0573-5

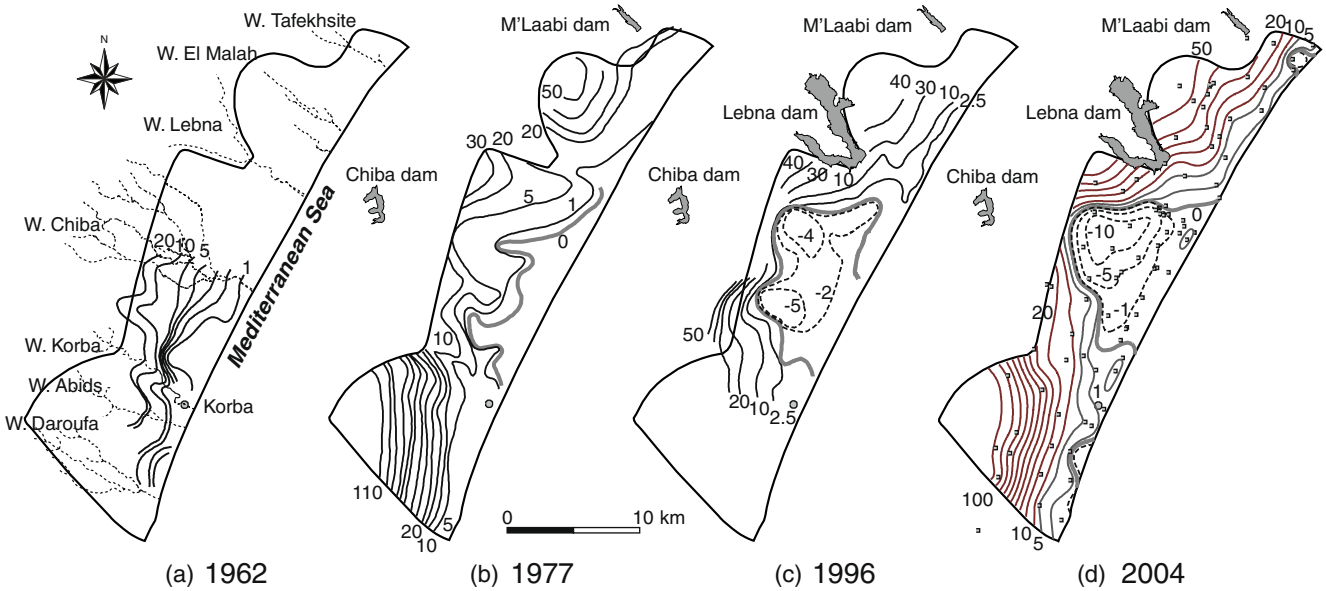

Fig. 2 Piezometric evolution [m.a.s.l.]: **a** 1962 from Ennabli (1980); **b** 1977 from Ennabli (1980); **c** December 1996 from Paniconi et al. (2001) and **d** August 2004. Contour intervals are not standard and the *0* sea reference iso-contour is represented by the *thick gray line*. The hydrological network is depicted by *dotted lines* and the dams by *gray shaded areas* (*Chiba* built in 1963; *M'Laabi* built in 1964 and *Lebna* built in 1986)

southern parts of the aquifer is that the water table is shallower in the Plio-Quaternary unit than in the Somâa making traditional implantation of wells easier.

In the following, the water balance of the Korba aquifer is presented starting with the inputs. The recharge of the aquifer by infiltration of precipitation is estimated to be less than 10% of the 420 mm/year average annual rainfall (Ennabli 1980; Paniconi et al. 2001). The integration of this value over the area of interest (400 km^2) yields 17 Mm^3/year. Additional recharge from wadis and topographic depressions is also expected. Note, however, that the most important wadis in the region, Chiba, M'laabi and Lebna (Fig. 2a) were dammed upstream in 1963, 1964 and 1986, respectively. Other wadis such as Korba (Fig. 2a), which drain a watershed of 85 km^2, have an average runoff of 3.7 Mm^3/year (Hichri 2003). Nazoumou (2002) estimated the infiltration from wadis in an arid area in the centre of Tunisia to be 30% of the annual runoff. According to that study, around 1.1 Mm^3/year will percolate from wadi Korba to the aquifer, 0.6 Mm^3/year from wadi Daroufa, 0.8 Mm^3/year from wadi Abids and 0.6 Mm^3/year from wadi El Malah (Fig. 2a). Artificial recharge in the region of Diar El Hojjaj (Fig. 1) by direct infiltration of surface water from dams or from the Medjerda Cape Bon canal started in 1999 but never exceeded 1 Mm^3/year (CRDA 2002). Other sources of recharge are irrigation return flow (believed to be important) and the lateral recharge by leakage (or through faults) from the underlying Miocene sandstones are not yet evaluated.

On the other hand, groundwater abstraction represents a major output. Indeed, the exploitation of the Korba aquifer began in the 1960s mainly for irrigation purposes, and reached 43 Mm^3/year in the 1980s. In 2000, the total groundwater exploitation was estimated to be about 50 Mm^3 with more than 9,000 active wells (DGRE 2000). It is worth noting that the number of wells is proportional to the number of farms. Regional groundwater is heavily exploited despite the efforts of the government to mobilize most of the regional surface water and to transport water from the north of the country via the Medjerda Cape Bon canal. Moreover, in the beginning of the 1990s, the government encouraged the farmers to adopt drip irrigation systems by contributing 60% of the cost of the installation in order to reduce water consumption. The result was that irrigated surfaces increased at the cost of the same water consumption. The *sebkhas* (salt lakes) forming a 5 km^2 strip all along the coastline, are suspected to be a groundwater discharge areas. Other outputs like submarine groundwater discharge (SGD) are not yet evaluated.

The previously mentioned incoming magnitudes allow estimating the total recharge in steady state and in the absence of pumping (before 1960). This is of the order of 25 Mm^3/year, which represents mostly the SGD. The total abstraction nowadays represents about twice the amount of recharge. Even without a precise estimation of the other components of the groundwater mass balance, it is self-evident that current overexploitation results in a depletion of the water table and a reduction of the SGD, which leads to an increase of seawater intrusion.

Piezometry and seawater intrusion characterization

Three piezometric maps and salinity data are available (Ennabli 1980; Khlaifi 1998; Paniconi et al. 2001). Figure 2 displays the evolution of the piezometric level in the Korba aquifer from 1962 to 2004 as well as the hydrographic network (Fig. 2a) and local dams according to their construction period. The piezometric maps of 1962 and 1977 (Fig. 2a,b) show that there was a reduction

 DOI 10.1007/s10040-010-0573-5

of the hydraulic heads in the Korba aquifer to below sea level after 1977 (most likely a few years later in the 1980s when aquifer exploitation reached 43 Mm^3). A visual comparison of Fig. 2a,b shows that damming wadi Chiba in 1963 caused a decrease of the water table downstream due to a reduction of recharge by its effluents. In addition to the perturbation of surface water regime, the growth of groundwater abstraction during the 1980s (51.5 Mm^3 in 1985), especially near the coast, lead to the apparition in 1996 of a concentric depression of 5 m below (Fig. 2c) sea level in the region of Diar El Hojjaj. This means that the hydraulic gradients were reversed mainly toward the central part of the aquifer leading to an acceleration of seawater intrusion. Indeed, hundreds of wells close to the coast were salinized and then abandoned despite the action of the government forbidding new wells in the area and distributing surface water. Years after, the depression of Diar El Hojjaj was attenuated and even disappeared; however, pumping migrated northward and led to the apparition of a critical depression of 12 m below sea level in 2004 (Fig. 2d). As opposed to the Chiba dam, the Lebna dam (constructed in 1986) had a positive effect on the aquifer recharge (compare Fig. 2b,d). Figure 2 also shows that the interaction between wadis and the aquifer has been perturbed. Using an average porosity of 0.12 (Ennabli 1980) and the depletion of heads from 1962 to 2004, it is possible to estimate that the total volume of groundwater stored in the central part of the Korba aquifer was reduced by 100 Mm^3.

Obviously, the salinity distribution in the Korba aquifer is correlated with the piezometric evolution. The vertical salinity profiles measured in August 2004 allowed to delineate a 3D distribution of salt concentrations in the aquifer by ordinary kriging (Fig. 3a). This facilitates a qualitative description of the state of the resource. These data also permit to describe the evolution of the seawater intrusion by comparing them with data from 1996 (Fig. 3b,c). The 3D map of the electrical conductivity displays a wide mixing zone which is clearly affecting the region of Diar El Hojjaj in the central part of the aquifer. The same figure also shows vertical salt-water up-coning near points 3 and 4 (Fig. 3a). In 2004, the well IRH No. 11186 (No. 4 in Fig. 3), at 1.55 km inland presented TDS values ranging between 7 and 25 g/l, confirming the inland seawater encroachment. Based on data from 1996 and 2004, at points 4 and 5 separated by around 1 km, and considering a 0.5 relative concentration (the relative concentration is defined as the ratio between measured concentration in the aquifer and the concentration of dissolved salts in seawater), a minimum seawater intrusion velocity in the Korba aquifer is approximately 100 m/year.

Another feature arising from the 3D salinity map is the effect of the Lebna dam which allowed for the maintance of high heads and low salinity of groundwater in its surroundings, due to the large volumes infiltrated into the aquifer. In the same figure, it can also be seen that salt recycling plays a role in the salinization of the aquifer (Milnes and Renard 2004) far from the sea (see around

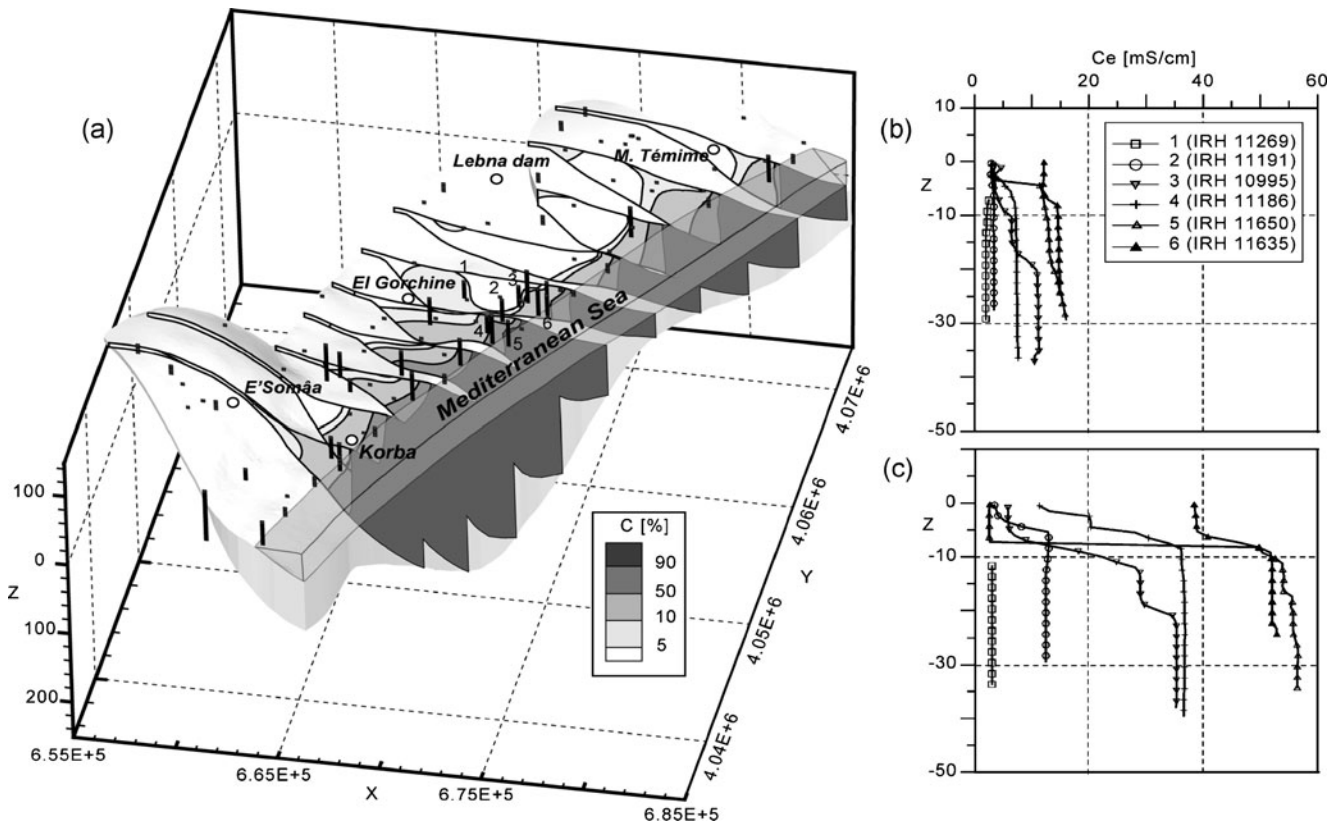

Fig. 3 Salinity description: **a** three-dimensional kriging of 854 data points; August 2004 vertical logs and surface measurements are represented by *black squares* or *black bars*; **b** vertical salinity logs of December 1996; **c** vertical salinity logs of August 2004. *Z* stands for elevation

 DOI 10.1007/s10040-010-0573-5

Gorshine and upstream in Fig. 3a). Grava (2005) showed that there is a strong correlation between nitrate (NO_3) and chloride (Cl^-) concentrations, meaning that irrigation return flow is accelerating the salinization of the aquifer.

The Korba aquifer numerical model development

In view of existing data and prior studies, there are still many unknowns concerning the behaviour of the Korba aquifer. Moreover, the components of the regional groundwater mass balance remain uncertain or unknown. Developing a new 3D numerical model will help to integrate all existing knowledge and data on the Korba aquifer for a better understanding of its dynamics and eventual use as a solid basis for the design of management policies. This section is organized as follows. First, the ingredients for building a conceptual model are presented. Next, the conceptual model is detailed (section Synthesis and conceptual model). Details on the numerical model are presented in section The 3D numerical model. Finally, the model calibration procedure is summarized in section Model calibration.

Model parameters

Aquifer geometry

The geometry of the reservoir is rather well known. Data from different sources: the work by Ennabli (1980), recent borehole lithostratigraphic logs and oil well logs; were combined to delineate the main aquifer formations and were used to interpolate by ordinary kriging the bedrock topography (Figs. 1, 8 and 9). In addition, a digital elevation model (DEM) was interpolated by ordinary kriging high-resolution data provided by the Tunisian Institute of Topography. The DEM was combined with the piezometric map of 1962 to build a hypothetical distribution of hydraulic heads in 1960. The latter was used as the top layer of the numerical model and for the calibration of the steady-state regime. Both the bedrock and the steady-state head maps allowed for the computation of a map of the saturated aquifer thickness, and, therefore, of the aquifer geometry. This is not only important for the groundwater flow (e.g. for the integration of the hydraulic conductivities) but also for transport simulations to accurately estimate groundwater volumes. The resulting average saturated thickness is estimated to be about 40 m.

Flow and transport parameters

In addition to the qualitative classification of the permeabilities described in section Regional hydrogeology, transmissivity data from 53 (short-term) pumping tests were provided by the local water management authority. These arise from conventional interpretation (i.e. assuming a homogenous medium) of drawdown data. Transmissivity data, unequally distributed over the aquifer, were first classified by formation and then transformed in terms of hydraulic conductivities using the whole saturated thickness of the aquifer for fully penetrating wells and the length of the screen for the others. This resulted in 16 permeability data for the Pliocene formation and 37 for the Somâa one.

The geometric mean hydraulic conductivity and the variance of the natural logarithm of Pliocene hydraulic conductivities are $8.9\ 10^{-5}$ m/s and 0.67, respectively, and $1.1\ 10^{-5}$ m/s and 1.6 for the Somâa sands. Those data show that the Somâa formation is more heterogeneous than the Pliocene one. At the same time, average values of hydraulic conductivities as well as their variance are probably biased because wells were most probably drilled in the highest transmissivity zones. Yet, the interesting point is that permeabilities of Pliocene sands are (on average) one order of magnitude larger than those of the Somâa sands. These estimates will be used initially as guesses for the calibration of the model.

With regard to transport parameters, there are no tracer test data to allow for the estimation of local dispersivities. However, high-resolution electrical resistivity tomography (ERT) was used to estimate the porosity of the Pliocene formation. The relationship between bulk resistivity of a fully saturated porous medium (ρ_r [Ohm-m]), its porosity (ϕ [-]) and the resistivity of the fluid within the pores (ρ_w [Ohm-m]) is expressed by Archie's law (Archie 1942):

$$\rho_r = a\rho_w \phi^{-m} = F\rho_w \quad (1)$$

where m and a are dimensionless material-dependent empirical factors; m is known as the cementation index; and F is the Humble formula (Winsauer et al. 1952)

Eight ERT profiles of 3–5-m electrode spacing investigating a depth of 30–50 m (approx. one-sixth of the total horizontal length) were carried out in the Pliocene area. Near each profile, there is a well where groundwater salinity was measured to estimate ρ_w. Figure 4 shows an example of an ERT profile with the corresponding borehole lithology and salinity profiles used for porosity estimation. ERT profile of point 4 shows the geological setting close to the sea with dry arenitic limestone of resistivities ranging between 10^3 and 1.5×10^3 Ohm-m on top of a saturated sand of 100–500 Ohm-m. Those offer a good contrast with the low resistivities (1–50 Ohm-m) of the clayey bedrock saturated with saline water. Results of applying Eq. 1 assuming Humble formula (Winsauer et al. 1952) for unconsolidated formations: $F = 0.81\phi^{-2}$ are displayed in Table 1 and show that the porosity of the Pliocene formation ranges between 4 and 25%. It is worthwhile noting that, except for point 4, only values at the level of the water table were used for calculating the porosity. Therefore, only a portion of the material is accounted for in the calculation.

Areal recharge

Evaluation of effective recharge is challenging in arid and semi-arid regions. Scanlon et al. (1997) pointed out the wide variability of some published values under similar climatic conditions. In addition, in such an intensively

 DOI 10.1007/s10040-010-0573-5

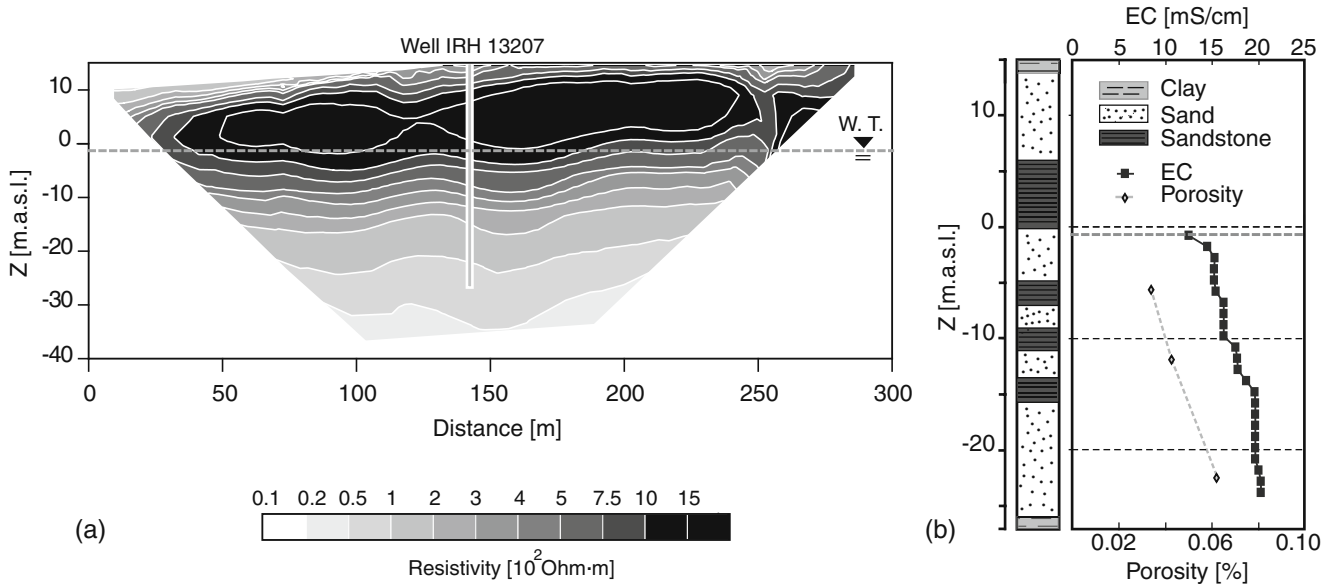

Fig. 4 **a** Inverted resistivity profile and location of the well and of the water table (*W.T.*); **b** Point 4 (*IRH 13207*) borehole data showing the local lithologies and the vertical salinity and porosity distributions calculated using Eq. 1. *Z* stands for elevation

irrigated plain as in Korba, irrigation return flow might be an important component of the groundwater mass balance. The study area is characterized by a semi-arid climate with an average precipitation deficit (precipitation minus pan evaporation) of around 650 mm/year. Generally, 75% of the 420 mm/year average rainfall is concentrated during the wet season (from September to March). Ennabli (1980) estimated the effective recharge rate as ranging between 5 and 8% of the regional average annual rainfall. Paniconi et al. (2001) estimated the effective recharge to be less than 10% of the average annual rainfall.

In this study, aquifer recharge was estimated using two different but complementary methods. The first method is based on the relationship between the effective recharge and the soil distribution in the area. The second method consists of the calibration of the recharge using a numerical groundwater model (section Model calibration). The following is a description of the first approach. The spatio-temporal analysis of the effective recharge by infiltration of precipitation was achieved using a geographic information system (GIS) database (including detailed soil and land cover maps as well as daily rainfall and pan evaporation data over 44 years) and the "daily" Thornthwaite and Mather method as described in Steenhuis and Van Der Molen (1986).

The regional soil distribution map (Mami and Aloui 1982) was discretized into 328,000 cells of 100 × 100 m. Three types of soil were defined: fine (F), medium (M) or coarse size (G) material. Each of these can have five possible thickness values: 40, 60, 80, 100 or 120 cm. This information on soil type distribution and thicknesses is of prime importance for the estimation of the soil water balance. To estimate the latter, one additionally needs the specific field capacity for each type of soil and climatic data. For the field capacity of each soil type, a sensitivity analysis was performed assuming three possible values for each one [%]: 5, 6.5 and 9 for the type G; 7, 8.5 and 11 for the type M; and 9, 10.5 and 13 for the type F. Note that for urban areas (U type) higher values (Fig. 5a) were used (15, 17.5 and 21%). Using soil type, its thickness and the corresponding specific field capacity, one can integrate a relative soil-class field capacity. This was used together with the daily rainfall and pan evaporation, to calculate the soil water balance, finally yielding the effective recharge. Average values were used during data gap periods. Figure 5a shows the values of the relative field capacity for each soil type. It is worth noting that surface runoff was neglected because of the flat topography and the dominance of cultivated areas.

Figure 5b shows the resulting recharge in terms of annual rainfall percentage. Indeed, minimal values of field capacity

Table 1 Measured resistivities and porosity values estimated by Archie's law, being a=0.81 and m=2

ID	X	Y	ZVAL	Bulk-media resistivity [Ohm-m]	Pore water conductivity [mS/cm]	Porosity [%] for a=0.81, m=2
1	673727.47	4071595.65	54.21	44.09	2.85	25
2	675403.99	4068851.79	12.72	54.17	2.7	24
3	673500.69	4070869.32	47.49	56.12	2.65	23
4	670454.79	4058971.23	15.00	416.26	13	4
5	665274.21	4062304.47	30.67	74.24	2.65	20
6	669843.62	4059709.35	16.73	65.02	5.29	15
7	675400.07	4071945.70	38.79	75.19	2.57	20
8	669694.83	4060084.50	20.00	62.9	5.00	16

 DOI 10.1007/s10040-010-0573-5

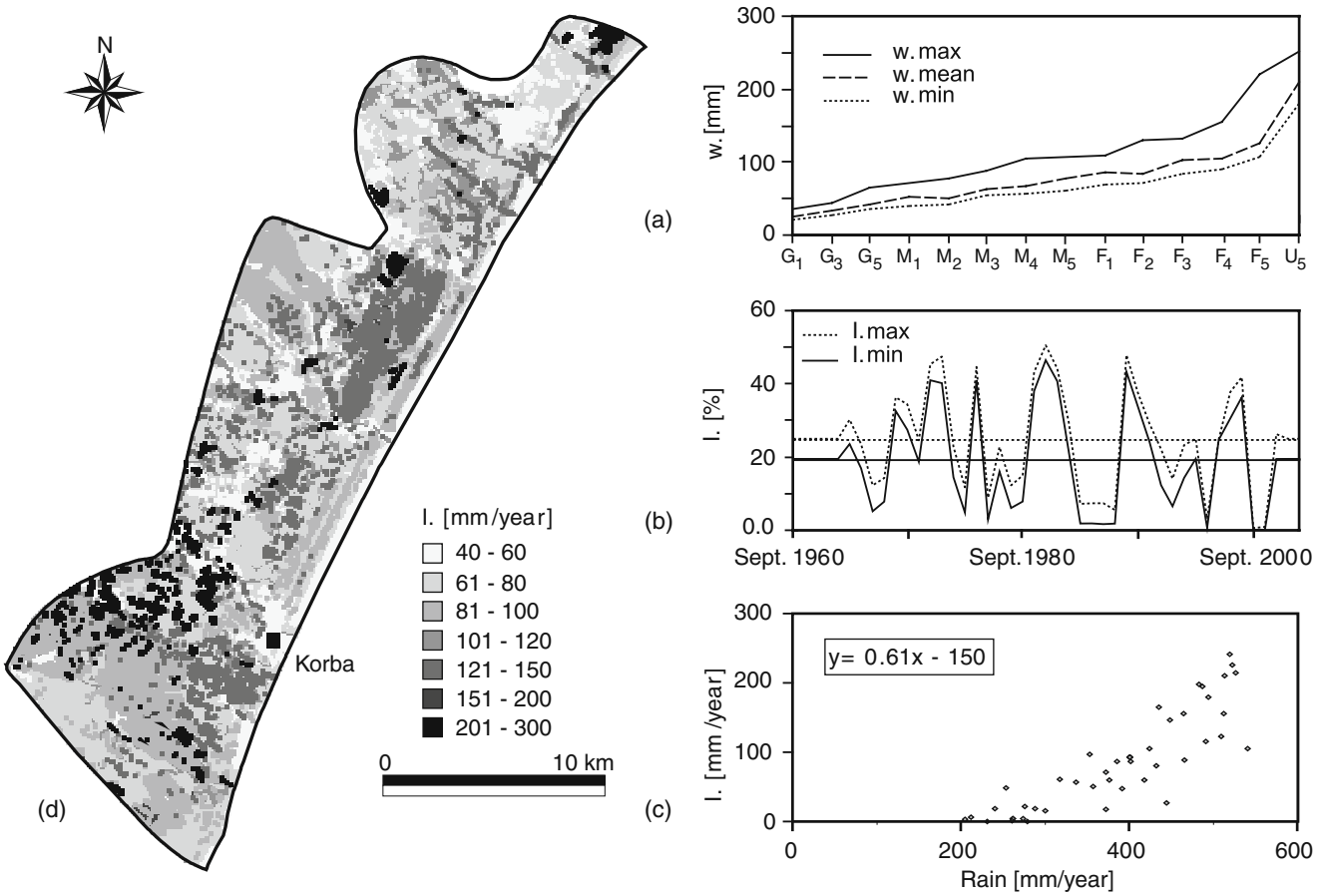

Fig. 5 Spatio-temporal analysis of the recharge at the Korba aquifer by infiltration of precipitation: **a** specific field capacity (*w*) of each soil type (the *letters* correspond to soil types: *F*ine, *M*edium, and *C*oarse. The *subscripts 1–5* correspond to the thickness of the soil (40, 60, 80, 100 and 120 cm), example: G_1: G type with 40 cm thickness; **b** The percentage of the annual rain that percolates to the aquifer (*min*, *max*); **c** Correlation plot between predicted recharge (*i*) and annual rainfall; **d** spatial distribution of the recharge data

and soil thickness lead to the maximal recharge scenario with up to 25% of the annual rain. In the following, only the minimal recharge scenario was considered. The recharge at the Korba aquifer ranges on average between 8 and 30% of the annual rainfall depending especially on the frequency and the intensity of the rainy events during the year. However, below an annual rainfall of 200 mm (Fig. 5c), no recharge will occur or it will be negligible, as was the case during the period of 1985–1988 (Fig. 5b). Such long drought periods may favour seawater intrusion.

An important result of recharge analysis was the spatial variation of the recharge rate which may vary by one order of magnitude (Fig. 5d). A total of 90% of the recharge takes place during the wet season and the inter-annual variation of the recharge might be more than 2.5 times the average value (Fig. 5b). These estimated values of recharge are surprisingly high when compared to those in previous studies. This is partly explained by the method (Thornthwaite and Mather) and the temporal discretization used (daily or monthly). This may lead to a systematic under-estimation of recharge in case of monthly time steps because of the dominance of the evaporation in such semi-arid contexts.

Irrigation return flow was also estimated using the previously mentioned data, and additionally using data from land cover analysis of 1998 and a detailed irrigation calendar. The irrigated volumes were added to the rain and the same method was applied. The amount of irrigation water which percolates to the aquifer might increase the total recharge by 8 Mm^3 (on average) per year, which represents 16% of irrigation water (assuming 50 Mm^3). Note that the analysis of return flow irrigation was made for just 10 years (1993–2003) assuming a constant land-cover distribution.

The previously estimated average annual recharge will be used as an initial guess for the inverse modelling of the steady-state flow (section Model calibration). Its variation rates will be used for the transient simulation using a simplified zonation according to geological criteria which also control aquifer recharge.

Sink terms

The sebkhas delineate a 5 km^2 fringe all along the coastline and are believed to be groundwater discharge areas. Appling the empirical formula of Coudrain-Ribstein et al. (1998) and considering 0.5–1.5 m depth of the water table gives a 0.8 Mm^3/year discharge in average. Thus, this value is negligible. Other sink terms like submarine groundwater discharge are not evaluated. In the following,

 DOI 10.1007/s10040-010-0573-5

focus was on the estimation of the pumping rates, which are the key to understanding the aquifer dynamics, modelling seawater intrusion, and investigating optimal groundwater-management strategies.

Data for the estimation of pumping rates. Different types and sources of data were used to estimate a map of extraction rates. First, global estimates of the total annual extraction (Q_{annual}) are regularly made by the local administration (CRDA Nabeul). This calculation is based on average seasonal head variation and estimated aquifer porosity. As such, it is not very precise. Eight such values are available starting from 1962. According to these records, pumping started in the 1960s and increased regularly up to the mid-1980s. Since then, the exploitation rates oscillate around 50 Mm^3/year. The stabilization can be explained, on the one hand, by the change from flood irrigation to drip-irrigation and, on the other hand, by the construction of a network of surface water supply for irrigation in some parts of the study area. The uncertainty around these estimated groundwater abstraction volumes has never been evaluated.

However, a thorough survey of pumping rates was conducted in 1996 jointly by the Institut National Agronomique de Tunisie and the CRDA Nabeul. During this survey, 432 sites were visited. Farmers were interviewed and the instantaneous discharge rates were measured. From the declaration of the farmers with regard to water usage, the type of crops they grew and the measured pumping rates, an annual value of the pumping rates for the well 'i' was estimated at selected wells. These are located in the central part of the aquifer (Fig. 7a). This data set constitutes the best source of information for evaluating the spatial variability of pumping rates and their relation with background variables. Thus, they are considered as reference values even when they (certainly) also contain some uncertainty.

The main assumption while estimating the pumping rates distribution is that extraction correlates with exhaustive secondary information available over the whole domain. For example, it is reasonable to think that the pumping rates distribution is related to the density of wells and proportional to the transmissivity of the aquifer, etc. The location of shallow and deep wells in 1996 was provided by the CRDA. From that data set, the density of wells was calculated over a regular grid of 300×300 m resolution (Fig. 7a). The pumping rates estimated by the exhaustive survey in the central part of the aquifer were integrated as hard data on the same regular grid. Other variables were directly available and some had to be computed a priori. In particular, the next section presents how crop evapotranspiration and its spatial distribution were obtained using energy balance calculation on satellite images.

Mapping crop evaporation by remote sensing analysis. Remote sensing can be extremely efficient to acquire spatially distributed data for modeling (Becker 2006; Brunner et al. 2007; Hendricks Franssen et al. 2008). Considering the problem of the estimation of the pumping rates, one technique consists of estimating the crop evaporation from energy balance computations (Bastiaanssen et al. 1998a; Bastiaanssen et al. 1998b; Roerink et al. 2000; Anderson and Kustas 2008) and use that estimation to derive pumping rates from the water mass balance.

For this purpose, the Simplified Surface Energy Balance Index (S-SEBI) algorithm (Roerink et al. 2000) and the equation of Penman-Montheith (Allen et al. 1998) were used (Käser 2004). In all, 23 cloud-free satellite images NOAA AVHRR (advanced very high resolution radiometer) were selected between the 14th February 2000 and the 15th September 2000. Each image has a 1.1-km^2 resolution. The data set also includes air temperature and relative humidity measured on the site by two meteorological stations. First, the 5-band images were processed to calculate surface reflectance (ground albedo) and surface temperature which are two constitutive parameters for the S-SEBI algorithm. It assumes that the atmospheric conditions are constant over the image and the area reflects sufficiently wet and dry pixels. This was the case in the eastern part of the Cape Bon images. Then, the instantaneous evaporative fraction was calculated for each pixel on the basis of the expression of ground albedo versus surface temperature as described in Roerink et al. (2000). Second, using air temperature and relative humidity maps, the daily net radiation was calculated, which in turn was used to compute the daily evapotranspiration as described in Parodi (2002). The daily evapotranspiration allowed estimating the crop reflectance coefficient using the reference evapotranspiration ET_0, calculated by the Penman-Montheith equation, and provided by the Tunisian Institute of Meteorology. The crop reflectance coefficient was then averaged for each month and used with the reference evapotranspiration to calculate seasonal evapotranspiration ET_r over the whole aquifer.

To estimate the pumping rates, the basic assumption is that the difference of ET_r between not irrigated and irrigated areas represents the water that has been added by irrigation and can be subdivided into a surface water and pumped groundwater (Fig. 6b).

The estimated values of evapotranspiration are 45 mm/month in July and 57 mm/month in August for the non-irrigated area and 62 and 71 mm/month for the same months respectively, in the irrigated area. Figure 6a shows the crop evaporation of 25th June 2000. The mean difference in ET_r is therefore 14.5 mm/month. Assuming that the pumping rates are constant all along the year over the 168.5 km^2 of irrigated area, and knowing that the amount of surface water used for irrigation was 9 Mm^3 (CRDA 2002), the pumping volume for the year 2000 is estimated to be around 18 Mm^3. This value is much smaller than the estimate of 50 Mm^3/year provided by the local authority and therefore seems to be underestimated (even if 8 Mm^3/year of irrigation return flow are added). This might be explained by the low resolution of the used satellite images (1.1 km^2) which leads to an underestimation of the crop reflectance coefficient. The reso-

 DOI 10.1007/s10040-010-0573-5

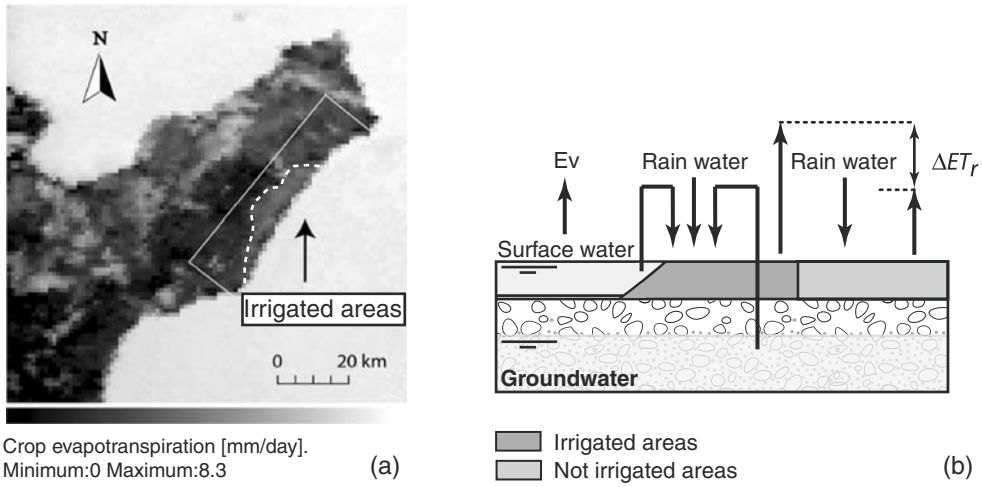

Fig. 6 **a** Crop evapotranspiration for the date of 25 June 2000 modified after Käser (2004). The irrigated area delimited with a *dashed white line* is also shown. **b** Sketch of the model for estimating pumping rates

lution problem is related to the fact that farmers have very small fields. The surface of 72% of the farms is less then 5 ha (CRDA 2002), and use mixed multilevel agriculture in the same plot. This introduces a high variability within the pixels of the satellite images. Another source of error could be an inadequate calibration due to a lack of reference ground data. However, even if the absolute value of the estimated evaporation does not seem sufficiently reliable, it is reasonable to think that the method allows for the identification of regions with higher evapotranspiration and, therefore, higher pumping rates.

Multi-linear regression model for the pumping rates. Pumping rates are assumed to be partly correlated with secondary information available over the whole domain. For example, groundwater abstraction is assumed to be related to the amount of crop evapotranspiration and its spatial distribution calculated using remote sensing analysis. In addition, pumping rates are expected to be correlated with parameters such as: transmissivity (high transmissivity allows high discharge) or depth of the water table (shallow depth facilitates groundwater abstraction). The pumping rates might also be related to other parameters such as: (1) the salinity of the groundwater: if the salinity increases, the groundwater will no longer be suited for irrigation; thus, pumping will decrease or eventually stop; (2) the elevation of the topography: at higher elevation, the water table is deeper, which makes traditional well digging more difficult and therefore less pumping is expected; (3) the distance to the sea: far inland the water is less saline; (4) the seasonal piezometric head variation in 1996 indicates the areas with larger stress (5) the piezometric depletion since 1960 indicates the most exploited areas in the long term.

Overall, eight parameters were selected as potential secondary information (Fig. 7b). These are: aquifer transmissivity (T), summer 2000 crop evapotranspiration (ET_r), December 1996 electrical conductivity (Ce), 1996 seasonal head variation (Dh_{96}), average 1996 water-table depth (WT_d), 1960–2004 historical piezometric decline (Dh_h), distance to the sea (D_s), and digital elevation model (Z). For each of these parameters, a distribution map was either already available or it was constructed by ordinary kriging.

Pumping rates measurements at 432 wells (within the dashed polygon in Fig. 7a) were used as hard data to estimate the coefficients of a linear multivariate regression model. In a first step, the pair-wise correlations between the selected parameters and measured pumping rates were analyzed (Fig. 7c). Some correlations are weak, as for example the correlation between the pumping rates and the distance to the sea or the altitude, but some others are statistically significant (with the transmissivity and with the average seasonal head variation). There was also a clear trend between the pumping rates and crop evapotranspiration of 2000 despite the time lag. In a second step, a multi-linear model was estimated by standard linear least squares. The correlation coefficient values obtained by regression reveal that the agreement between interpolated and measured pumping rates is poor (Fig. 7d). Yet, results of the linear regression model are taken simply as initial guesses for the numerical model (section The 3D numerical model and Model calibration). These will be updated by model calibration in such a way that a good agreement with available (head and salt concentration) calibration data is achieved.

Synthesis and conceptual model

Prior analysis of aforementioned data allows one to elaborate a conceptual model depicting the dynamics of the Korba aquifer (Fig. 8). This is the foundation of any subsequent numerical modelling endeavor (Carrera et al. 2005). The key points and assumptions in the conceptual model adopted here are listed below:

– Northern and southern limits match groundwater flow streamlines. Western limit depicts the contact with the early Miocene marls. Eastern limit matches the seashore.

 DOI 10.1007/s10040-010-0573-5

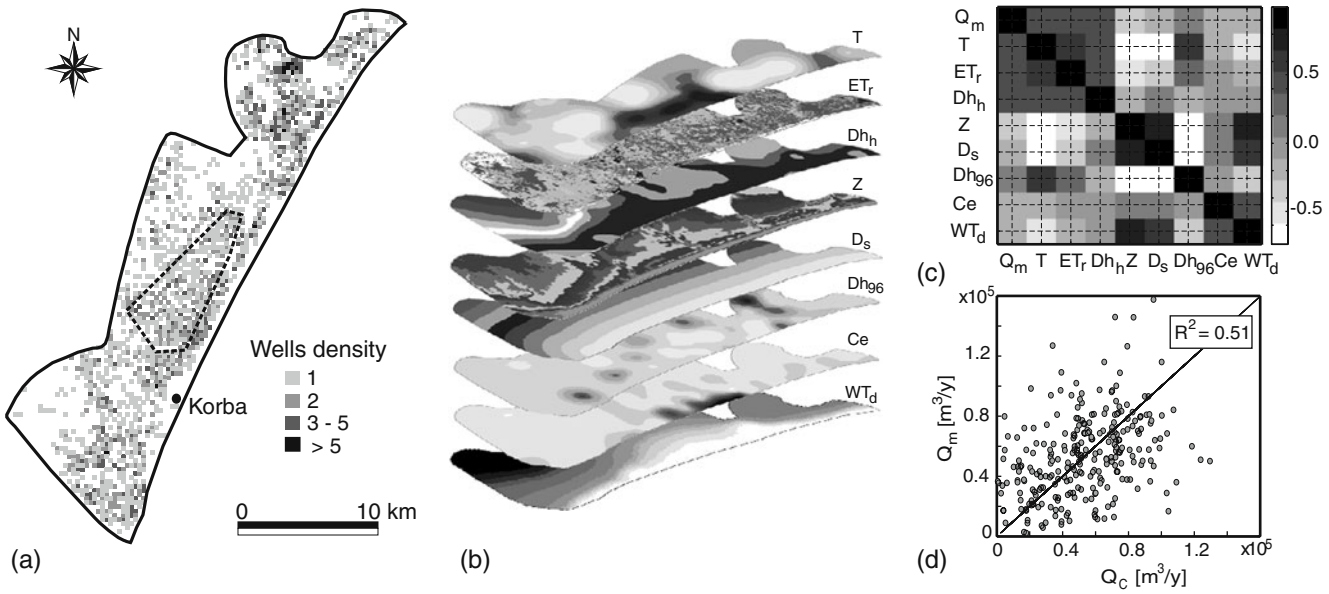

Fig. 7 **a** Wells density and area of the exhaustive pumping rate survey (*dashed line polygon*). Wells are grouped into 1,491 clusters on a regular grid of 300 × 300 m cell size. **b** Eight maps with the secondary information. The eight parameters are: aquifer transmissivity (T), summer 2000 crop evapotranspiration (ET_r), December 1996 electrical conductivity (Ce), 1996 seasonal head variation (Dh_{96}), average 1996 water-table depth (WT_d), 1960–2004 historical piezometric decline (Dh_h), distance to the sea (D_s), and digital elevation model (Z). **c** Correlation matrix. **d** Scatter plot of estimated (Q_c) vs. measured (Q_m) pumping rates

- Five geological units are considered (Figs. 8 and 9): the Tyrrhenian Quaternary (Q1); the marine Pliocene (P1) considered as the main aquifer; alluvial Pliocene in the central part of the domain (P2); late Miocene (the Somâa sands) in the southern part of the aquifer (M2); and the early Miocene (M1).
- Hydraulic parameters are considered homogenous in each of the aforementioned units considering the qualitative description (see section Regional hydrogeology) and available data (see sections Flow and transport parameters)
- The main groundwater mass balance inputs are areal recharge estimated to be about 20% of the average annual rainfall and vary in space and time. Lateral recharge and recharge from wadis are also considered.
- Groundwater abstraction is assumed to be started in the 1960s and increased linearly until the 1980s. Since the 1980s, the total abstraction volumes are assumed to fluctuate around 50 Mm^3/year (as described in section Sink terms).
- Figure 8 shows that the mixing zone is very wide in the Korba aquifer, on the order of several kilometers (in the central part of the aquifer, there is about 1.5 km between the 0.25 and 0.75 iso-concentration contours) with almost vertical salt iso-concentrations. It is obvious that, in this case, a sharp interface conceptual

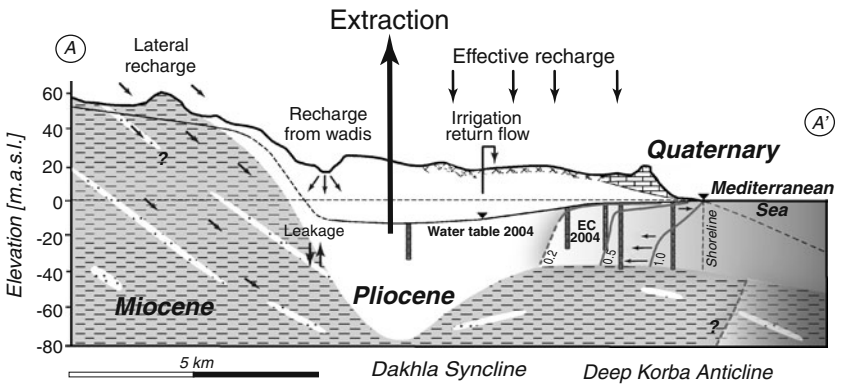

Fig. 8 Simplified geological cross-section (localization in Fig. 1) of the Korba aquifer system sketching the conceptual model based on up-to-date geological and hydrodynamic data. The aquifer surface and bedrock topography are shown as well as the August 2004 *water table* and the relative electrical conductivity of seawater (the maps are constructed by kriging). Note that *dashed line* iso-contours are hypothetical and the *question marks* mean that the extension of those units is not well known

 DOI 10.1007/s10040-010-0573-5

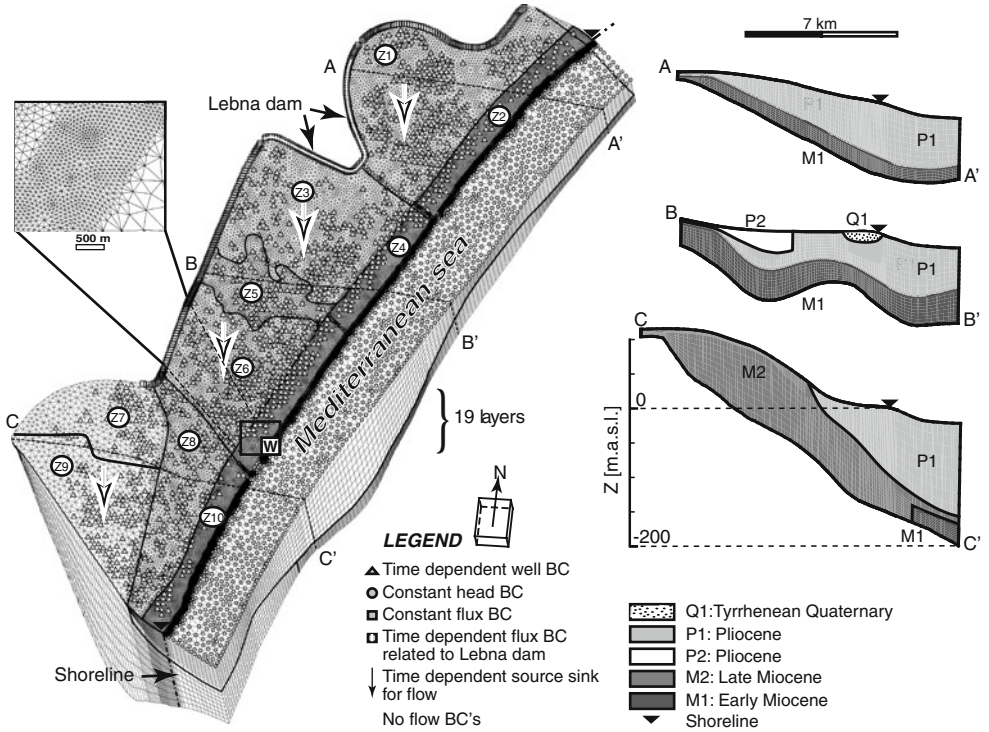

Fig. 9 The Korba aquifer 3D numerical model and three flow material cross-sections (*W* zoom window). Note that wells are attributed at the third slice and lateral fluxes are integrated on the thickness of the Pliocene only. The zonation (*Z1–Z10*) used for inverse calibration is also shown

model will lead to misleading results. Therefore, it is necessary to account for dispersion-diffusion processes.
– Given the variability of flow and concentrations patterns, a 2D numerical model will yield local predictions only. However, a 3D model will be suited to account for lateral changes of the hydrodynamic parameters of the aquifer as well as the forcing terms.

The 3D numerical model

The 3D numerical model (Fig. 9) was built using FEFLOW (Diersch 1996). The model domain was discretized in 877,249 prismatic finite elements and 467,760 nodes (Fig. 9). The mesh is refined within the main aquifer layer (Pliocene formation) with element sizes ranging from 150 to 200 m. Near the shoreline, element sizes range between 50 and 100 m. Vertically, the mesh is divided into 19 layers of 5 m thickness in average. The mesh setup involved a pre-processing of GIS data of different kinds: points (wells and piezometers), polygons and lines (geological units, wadis, etc.) and raster maps (geological layers, surface, top and bottom topography, etc.). According to the local geology data and soil distribution, the area is divided into 10 sub-domains (called zones) in which the model parameters are calibrated separately (Fig. 9). This increases the degrees of freedom of the model but allows, first, a more realistic representation of the aquifer geometry and, second, a better fit of available observations.

Modelling is performed in two steps. First, a steady-state flow model is used to estimate hydraulic conductivities and recharge, and get suitable initial conditions (heads and concentrations) for the transient model. The latter is performed in a second step and allows the estimation of storativity. Steady-state boundary conditions (BC) are a prescribed constant lateral inflow for most of the length of the western boundary and a prescribed head on the seafloor (Fig. 9). The seaside boundary extends 3.5 km (arbitrarily fixed) offshore to avoid unrealistic boundary effects. For the transient simulation from 1960 to 2004 time period, lateral fluxes were attributed to model recharge from the Lebna dam (from 1986), and the increasing discharge rates in the wells. Based on the eight estimates of total exploitation volumes and under the assumption that pumping started in 1960 and increased linearly up to 1980, a suitable time function is adopted at the majority of wells (e.g. well Q_{240} in Fig. 10b). Since pumping was greatly reduced north of Korba in the early 1990s (dashed line polygon in Fig. 10a) due to the high salinity, a second time-dependent function was built for the wells located in that region (e.g. well Q_{361} in Fig. 10b). Note that pumps are simulated at 10 m depth on average. The recharge of the aquifer by infiltration of precipitation (on the top layer of the model) varies in time (yearly) as shown in Fig. 5b. A total number of 1,498 time-dependent functions (1,491 for the well clusters, 6 for the areal recharge and 1 for the lateral flux) are considered for the transient simulations. With regard to transport boundary conditions, a maximum relative seawater concentration of 1 [-] was

 DOI 10.1007/s10040-010-0573-5

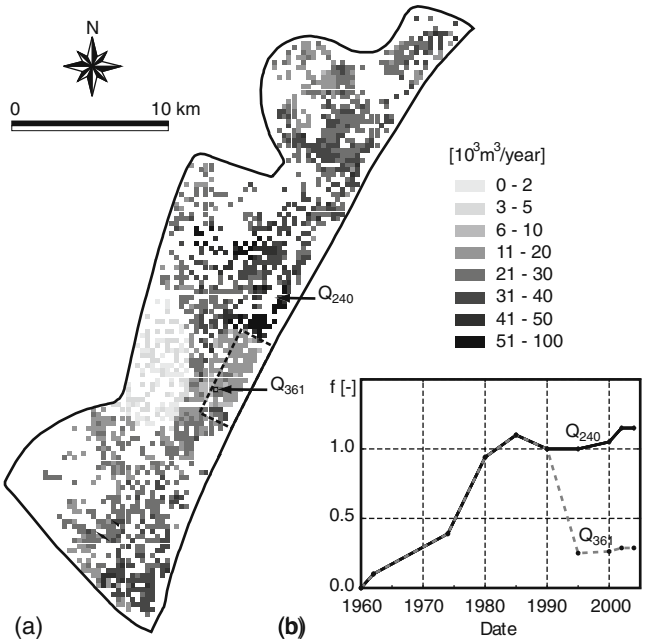

Fig. 10 **a** Average pumping rates (Q 1996) with the area (delineated with *dashed line*) where pumping was reduced in the 1990s. **b** Time-dependent evolution functions *f [-]* for both wells (*solid black line* for Q_{240} and *gray dashed line* for Q_{361}) with 1996 extracted volumes as reference

assigned at the seafloor to inward seawater fluxes only (water enters the aquifer with seawater concentration but leaves with aquifer concentration).

Model calibration

The calibration of the 3D model to fit field observations was achieved in a time dependent, iterative and semi-automatic fashion using PEST (Doherty 1998) coupled to FEFLOW. The basic idea of the PEST algorithm is the minimization of an objective function defined by the squared weighted sum of residuals (calculated minus observed heads). Model parameters to be calibrated were the geometric mean of the hydraulic conductivity of each formation, the spatial distribution of recharge and the lateral flux. The conditioning dataset for the steady-state calibration was that of 1960, presumably representing natural conditions. To run PEST safely, some constraints (spatial and numeric) have to be fixed. Based on a stratigraphic qualitative analysis, the Tyrrhenian sandstone was defined as the most permeable unit, followed by the Pliocene, the Somâa and the early Miocene formations. However, for recharge, the estimated average values plus and minus standard deviation were fixed as a tolerance interval. Note, however, that for all parameters, the calibration was carried out using 10 subdivisions of the domain to account for the local geology (Fig. 9).

PEST was then used to calibrate the storage compressibility using 1,753 time-dependent measured heads as control data (including monthly data during 20-years in six wells and 6-months data during 10-years in 21 wells history). When the resulting heads did not match the observed heads in 2004 sufficiently, then both permeabilities and areal recharge were recalibrated in steady state first by adapting their ranges (minimum and maximum admitted values for the inverse calibration). If this was still not sufficient, pumping rates estimated by the linear regression model were modified locally (especially near Korba city) and rescaled to fit the transient estimations given by the authorities and finally PEST was restarted again until convergence.

With regard to the transport calibration, tests were made by trial and error to get adequate horizontal and transversal dispersivities (constant in space). Values were chosen sufficiently large enough to avoid competition with numerical dispersion in the largest elements. Then, the porosities were also calibrated manually by trial and error with respect to local lithologies to reproduce as well as possible the 26 vertical profiles of salinity measured in 2004 as well as 80 shallow local salinity values.

Simulations results

The model was calibrated to reproduce the long-term depletion of groundwater levels and seawater encroachment by considering inter-annual variability of the recharge (Fig. 5b) and increasing pumping rates (Fig. 10b). In 1985 and 2004, the total estimated exploitation volumes were 50 and 47 Mm^3/year respectively, with an average pumping rate on a single grid cell of 3.37 and 3.15 10^4 m^3/year. The map of calibrated pumping rates (Fig. 10) shows that the pumping rates at the west of Korba are the smallest. This is related to the low transmissivities in that area of the aquifer.

Figure 11 shows the quality of the fit between observed and calculated heads and concentrations for the transient model. Root mean square errors of 6.2 [m] for heads ($-12 < H_{obs} < 120$ m) and 6.69 [g/l] for salt concentrations ($0.5 < C_{obs} < 36$ g/l) were obtained, indicating an acceptable calibration. A better fit could certainly be obtained by considering a heterogeneous hydraulic conductivity field, but the sensitivity analysis showed that it is difficult to get a better calibration with the conceptual model used. The calibrated parameters are shown in Table 2.

Figure 12 shows the simulated heads and relative concentrations of salt. They are in agreement with field observations (compare Figs. 2d and 12a and Figs. 3a and 12b and Figs. 8 and 12c) and reproduce the main hydraulic features of the aquifer including the highest gradients in the Somâa aquifer and water table depression in the centre of the aquifer. The model also allowed the quantification of the groundwater mass balance (Fig. 13) which will be discussed later. In addition, the model allowed for the reproduction of the lateral extension of the seawater intrusion, its time evolution and its extent in 2004 (Figs. 12b,c and 14). The vertical shape of the salt-water wedge is less well reproduced. This is a frequent problem in regional-scale 3D seawater intrusion models where the computed profiles are too steep as compared to the observed ones, which is due to the simplifications

 DOI 10.1007/s10040-010-0573-5

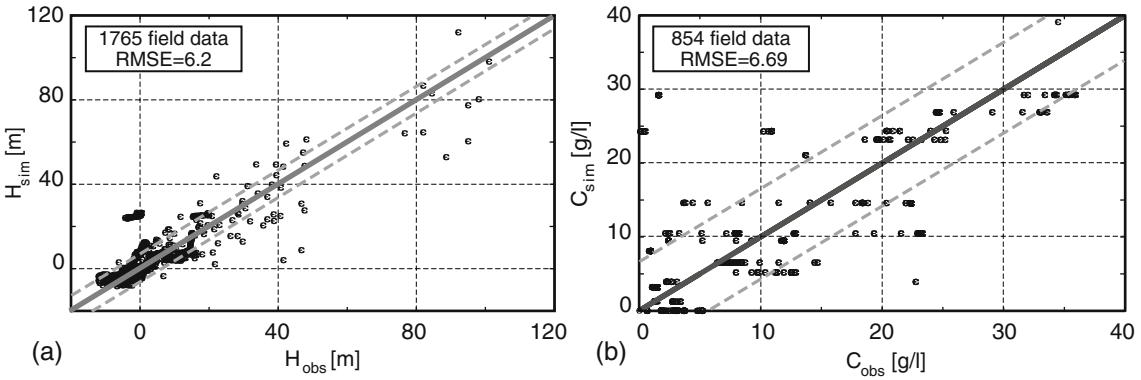

Fig. 11 Scatter plots showing the fit between the observed and calculated: **a** heads [m] and **b** salt concentrations [g/l]. In both cases, the *thick grey line* represents observed values = simulated values and *dashed grey lines* represent observed values ±RMSE. Note that 1,765 measured data points of August 2004 were used for heads and 854 measured data points were used for concentrations

(coarse vertical resolution: 5 m in average, homogeneous parameters) required at such a scale. Very often, in miscible salt transport models, the 0.5 relative seawater concentration is used to characterize the extension and the geometry of the salt-water wedge in analogy to sharp interface models. Yet, with such a wide mixing zone as the one in the Korba aquifer, it is misleading to use the 0.5 concentrations to characterize seawater intrusion. At the same time, using very low seawater concentrations (e.g. 1%) can also be misleading because of boundaries but also numerical effects.

In this study, the 0.25 and 0.75 relative concentrations are considered to define the width of the mixing zone and the 0.25 to define its extent within the aquifer. Obviously, salt-water wedge movement landward started in 1979 almost simultaneously with the decrease of the water table below sea level (Fig. 14). Most probably, migration of pumping wells inland as salinity increased above a certain threshold (as happened in the 1990s), led to further inland propagation of the salt-water wedge. The combination of reversed flow direction (hydraulic gradients) due to the depression of the water table below sea level and salt-water up-coning determined the velocity and the geometry of salt-water wedge in the Korba aquifer. In such a case, both horizontal and vertical dispersion coefficients increase proportionally to increasing directional velocities. The latter processes might explain the widening of the salt-water wedge at the same time as it is advancing (Fig. 14). From Fig. 14, the velocity of the salt-water wedge might be estimated to be around 100 m/year, considering the 0.25 concentration and 1.3 km width of the mixing zone in 2004 which represent 4 times the width of the mixing zone prior to seawater wedge encroachment. Figure 14 also shows that the velocity of the 0.25 iso-concentration accelerated in response to the decrease of the water table caused by increasing pumping stresses. However, at the same time as the velocity of the 0.25 iso-concentration increases, there is a slight decrease in the velocity of the higher iso-concentrations. This is normal, because salt spreading opposes density effects.

Table 2 Hydraulic proprieties. First, the deterministic proprieties are listed followed by calibrated model parameters (according to Fig. 9)

Parameter	Value
Seawater density [kg/m^3]	1.025×10^3
Freshwater density [kg/m^3]	1.00×10^3
Fluid viscosity [kg/m/s]	10^{-3}
Maximum relative concentration [-]	1
Average annual recharge [mm]	
Z1	164
Z2, Z4, Z10	73
Z3, Z5, Z6	43.8
Z7	45.6
Z8	54.7
Z9	119
Hydraulic conductivity (isotropic) [m/s]	
Q1; P1; P2 ;M1; M2	2×10^{-4} ; 1×10^{-4}; 5×10^{-5}; 6×10^{-6}; 1×10^{-7}
Storage compressibility [1/m]	
Q1, P1; P2; M1; M2	5×10^{-3}; 3×10^{-3}; 6×10^{-4}; 1×10^{-4}
Porosity [%]:	
Q1, P1; P2, M1; M2	10; 8; 5
Longitudinal dispersivity [m]	400
Transverse dispersivity [m]	40
Molecular diffusion [m^2/s]	10^{-8}

With regard to the groundwater mass balance (Fig. 13, Table 3), the mean areal recharge of the aquifer was estimated by model calibration to 29.7 Mm^3/year (89 mm/year) which is in agreement with the values obtained by the daily Thornthwaite Mather method (Fig. 9). Note, however, that on a major part of the aquifer (all zones except Z1 and Z9), areal recharge represents 12% of the annual average rainfall. Results show that infiltration is higher in the northern and southern parts of the aquifer where the main aquifers are outcropping (Z1 and Z9 in Fig. 9 and Table 2). The lateral recharge from the adjacent and deep aquifers as well as from the Lebna dam was estimated to be 7.5 Mm^3/year in 2004. The overexploitation induced an additional 7 Mm^3/year seawater inflow into the aquifer as compared to using steady state budget, while it caused a reduction of the submarine groundwater discharge of 16 Mm^3/year.

It is interesting to note that a transient simulation considering an average recharge constant over 44 years

 DOI 10.1007/s10040-010-0573-5

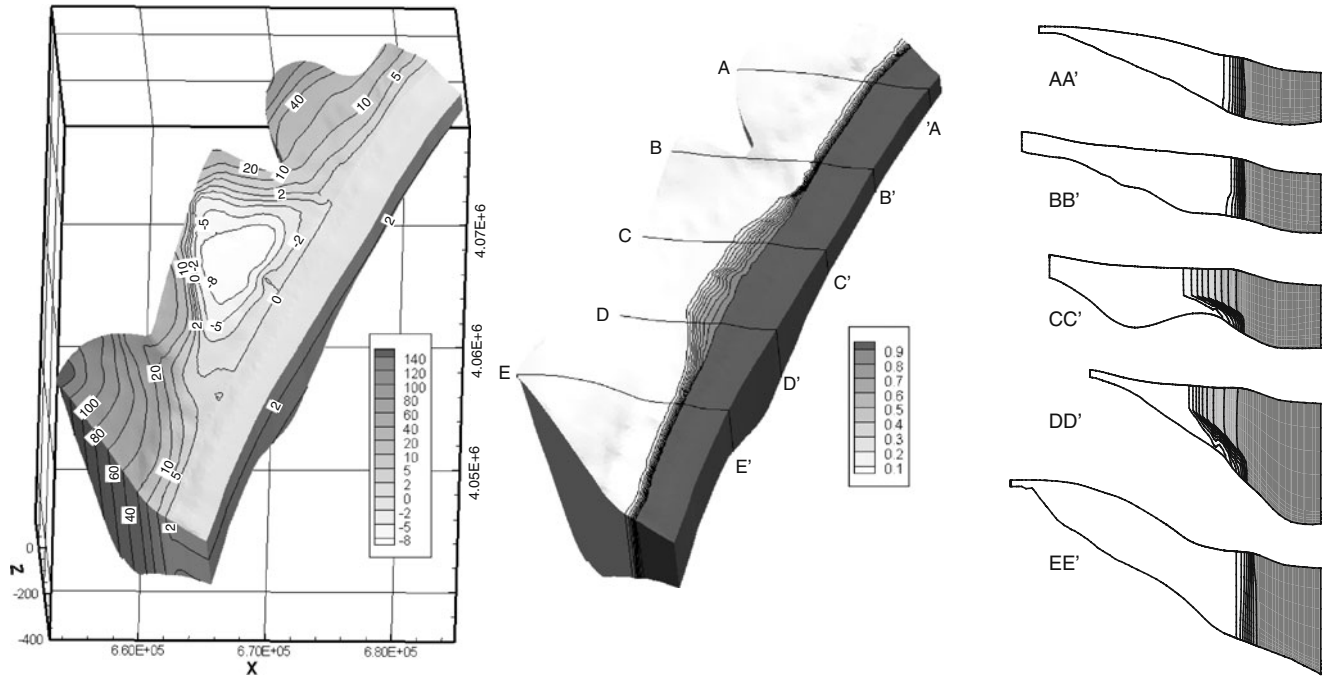

Fig. 12 **a** Three-dimensional views of simulated **a** water-table elevation [m.a.s.l.] with non-standard contour intervals; **b** relative salt concentration [-] distribution; **c** cross-sections

resulted almost in the same head and salt distributions as the simulation with time-dependent recharge and a 4-year drought period (e.g. 1985–1989) as shown in Fig. 13. This reflects the low diffusivity of the aquifer, especially the Pliocene formation, which is around 1.6×10^{-2} m^2/s.

Another way to evaluate the current situation of seawater intrusion in the Korba aquifer is the prediction of its evolution in response to pumping rate variations or even to a complete stop. The idea is to use the calibrated numerical model to evaluate the time lapse needed to turn back to the initial (steady state) head and salt concentration distributions. To this end, a simulation was conducted from 2004 to 2200 by keeping the same boundary conditions and aquifer recharge as in 2004 and turning off the pumping in the whole aquifer. A set of fictitious observation points with regular spacing, forming a line of 3 km perpendicular to the sea, were placed near the bottom of the Pliocene formation in the central part of the aquifer.

Figure 14 shows that the landward movement of the seawater wedge will persist another 10 years after turning off pumps. This is not surprising, because hydraulic gradients will take the same time to be reversed before groundwater restarts to flow towards the sea. The same figure also shows that the maximum width of the mixing zone is reached when salt-water started to recede with the same trends (velocity) for higher and lower iso-concentration. The 0.5 seawater iso-concentrations will take 80 years to turn back its initial position; however, 0.25 iso-concentration will take about 1.5 centuries; if, hypothetically, the pumping was turned off throughout the whole aquifer in 2004. Of course, these predictions are

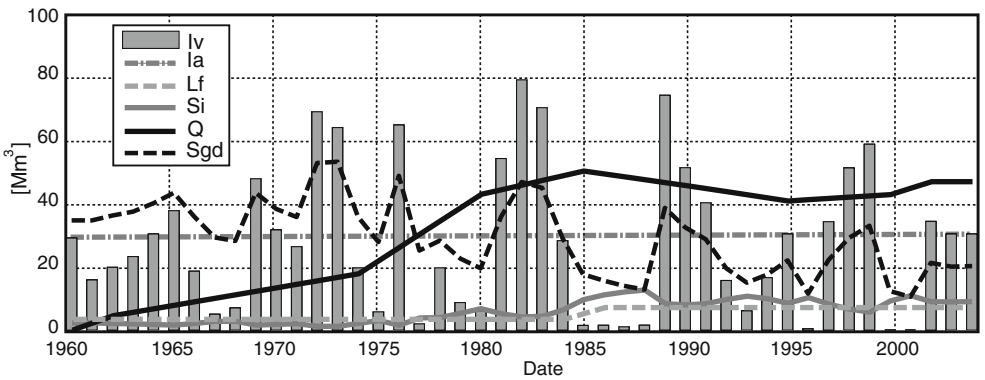

Fig. 13 Time evolution (1960–2004) of water budget in the Korba aquifer: *Iv* time dependent recharge, *Ia* average annual recharge, *Lf* lateral recharge with recharge from Lebna dam stating from 1986, *Si* seawater fluxes entering the system, *Q* pumping, *Sgd* submarine groundwater discharge

 DOI 10.1007/s10040-010-0573-5

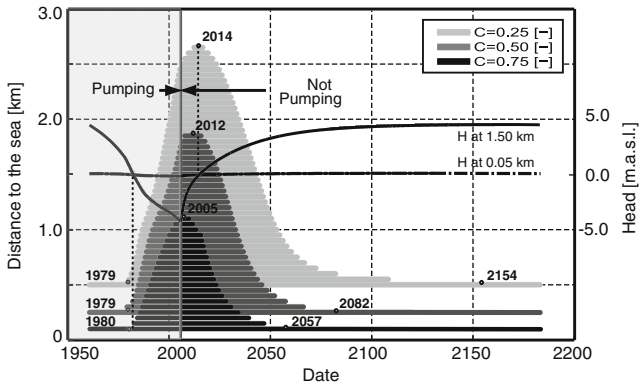

Fig. 14 Simulated seawater intrusion velocity from 1960 to 2004 considering actual pumping rates and the response of the aquifer to a hypothetical complete cessation of pumping from 2004

highly conditioned by the assumed boundary and initial conditions as well as hypothesis simplifying the conceptual model. However, it has been demonstrated that the shape of the bottom of an aquifer is a parameter that does have an effect on salt wedge penetration and geometry (Abarca et al. 2007). The bottom of the Korba aquifer is characterized by a landward slope of about 1–3° (Fig. 8). The latter configuration is believed to favour salt-water intrusion due to driven forces, while it is believed to oppose salt-water wedge recede seaward. Overall, the predictions made show that there is a long time lag that has to be taken into account to evaluate the effects of current regional groundwater resources depletion.

Discussion and conclusions

In order to address the current extent of seawater intrusion in the Korba aquifer, a large-scale three-dimensional numerical model of density-dependent flow and miscible solute transport was developed and reasonably well calibrated in a time dependent, iterative and semi-automatic manner. Some limitations of the model are due to the hypotheses that have been made and which are mainly related to the lack of available data. For example, assuming the same time evolution of the pumping rates (proportional to the global evolution) in the majority of the wells is certainly incorrect. Furthermore, the calibration of the model could certainly be improved by modeling the heterogeneity of the hydraulic conductivity field and by accounting for salt recycling (Milnes and Renard 2004). As for any modeling work, one issue is that the calibration procedure cannot guarantee the uniqueness of the solution. To ensure a reliable calibration (especially for the transient calibration), the value of the recharge was always controlled with care (to remain within a reasonable range) during the various iterations made between the calibrations in steady and transient regimes. Overall, the 3D model allowed not only for the accounting of the actual geometry of the aquifer, but also for the lateral variability of its physical properties as well as pumping and recharge. The prescribed boundary and initial conditions significantly control the calibrated model parameters and therefore the model outputs. Nevertheless, the regional flow features and their time evolution, the geometry of the mixing zone as well as the velocity of salt-water wedge are reasonably well reproduced.

Table 3 Groundwater mass balance of the Korba aquifer before exploitation (1960) and in 2004

	1960	2004
Average annual recharge [Mm^3/year]	29.12	30.40
Lateral recharge [Mm^3/year]	3.06	3.06
Recharge from Lebna dam since 1986 [Mm^3/year]	0.00	3.73
Seawater fluxes entering the system [Mm^3/year]	2.18	8.94
Pumping [Mm^3/year]	0.00	47.01
Submarine groundwater discharge [Mm^3/year]	34.72	19.98

The results show that the situation in the central part of the Korba aquifer is critical. A total of 135% of the recharge is exploited. The estimated pumping rates in the northern (north Lebna dam), central (between Lebna dam and Korba) and southern part of the Korba aquifer in 2004 are 13, 22, and 12 Mm^3/year, respectively; while the total recharge (areal and lateral) is 13, 10, and 14 Mm^3/year, respectively.

In addition, even if all the discharge were stopped now, the seawater would continue to further invade the aquifer for several years because, even if the head would progressively recover, it would take some time before the gradients would be reversed. The model allows for the estimation that it would take more than a century to recover a natural state. These results show a strong asymmetry between the time scale required to contaminate the aquifer (about 50 years) for the Korba aquifer and the time scale required for its natural remediation (150 years). This phenomenon is certainly occurring at various scales in other coastal aquifers in the world depending on the volume of the aquifers, their geometry, their hydraulic properties and the amount of natural recharge. In the Korba model, the phenomenon is also certainly underestimated because the model does not account for solute retardation in the aquifer and salt recycling due to irrigation that would also tend to fix the salt within the aquifer. Overall, the non-symmetry of the time scale is an important feature that authorities should account for when managing coastal aquifers.

The previous computations are not sufficient to define a sustainable exploitation rate, but they show that the current level of exploitation is not safe and not sustainable (Bredehoeft 2002). Management decisions have therefore to be taken to avoid further salt-water contamination, especially in the northern and southern part of the aquifer. A sustainable management scheme could be based on the 3D groundwater model developed in this study. This would require the development of a clear definition of acceptable and not acceptable impacts in the area, the collection of socio-economical data and the use of the model in an optimization framework.

Finally, the methodology that was used to estimate the spatial distribution of the pumping rates might also be applied in other locations and to estimate other model

 DOI 10.1007/s10040-010-0573-5

parameters. Natural recharge, for instance, can be estimated by combining secondary information like soil and geological maps, head and rain measurements as well as distributed data from remote sensing analysis in a statistical framework. However, there is still much to be done to improve the method by including, for example, principal components analysis (PCA) to better identify the secondary variables that influence the variable of interest or by using multivariate geostatistics using complex non-linear relationships.

Acknowledgements This work has been funded by the Swiss National Science Foundation under Grants: 207020-110017 and PP002-106557. Additional funds were provided by the Swiss Agency for Development and Cooperation and by the Institut National Agronomique de Tunisie. The authors thank G. de Marsily, R. Ababou, P. Perrochet, J. Carrera, R. Bouhlila and A. Alcolea for providing valuable suggestions on the manuscript. The authors are also grateful to Naceur Oueslati from CRDA Nabeul, and Emna Trabelsi from INAT who kindly provided the data.

References

Abarca E, Carrera J, Sanchez-Vila X, Voss CI (2007) Quasi-horizontal circulation cells in 3D seawater intrusion. J Hydrol 339:118–129

Abbes A, Polak M (1981) La formation Saouaf dans les synclinaux de la Dakhla (Cap-Bon) et de Saouaf (Tunisie nord orientale) [The Saouaf formation in the Dakhla (Cape Bon) and Saouaf (North-east Tunisia) synclines]. Notes Serv Géol Tunisie 46:99–111

Allen RG, Pereira LS, Raes D, Smith M (1998) Crop evapotranspiration: guidelines for computing crop water requirements. FAO Irrigation and drainage paper 56. FAO, Rome

Anderson M, Kustas W (2008) Thermal remote sensing of drought and evapotranspiration. EOS Trans Am Geophys Union 89:233–240

Archie GE (1942) The electrical resistivity log as an aid in determining some reservoir characteristics. Trans Am Inst Min Metall Pet Eng 146:54–61

Bastiaanssen WGM, Menenti M, Feddes RA, Holtslag AAM (1998a) A remote sensing surface energy balance algorithm for land (SEBAL): 1. formulation. J Hydrol 213:198–212

Bastiaanssen WGM, Pelgrum H, Wang J, Ma Y, Moreno JF, Roerink GJ, van der Wal T (1998b) A remote sensing surface energy balance algorithm for land (SEBAL): 2. validation. J Hydrol 213:213–229

Bear J, Cheng AHD, Sorek S, Ouazar D, Herrera I (1999) Seawater intrusion in coastal aquifers-concepts, methods and practices. Kluwer, Dordrecht, The Netherlands

Becker MW (2006) Potential for satellite remote sensing of ground water. Ground Water 44:306–318

Bensalem H (1992) Contribution à l'étude de la Géologie du Cap Bon: Stratigraphie, tectonique et sédimentologie [Contribution to the study of the geology of Cape Bon: stratigraphy, tectonic and sedimentology]. PhD Thesis, Faculté des Sciences de Tunis, Tunisia

Bensalem H (1995) Evolution de la Péninsule du Cap Bon (Tunisie nord-orientale) au cours du Néogène [Evolution of the Cape Bon peninsula (north-east Tunisia) during the Neogen]. Notes Serv Géol Tunisie 61:73–84

Bensalem H (1998) Les formations post Saouaf des environs de Nabeul (Cap Bon) et leur équivalents off shore et en Tunisie sud atlasique [The formations post Saouaf in the vicinity of Nabeul (Cape Bon) and their equivalents off shore and in south atlasic Tunisia]. Notes Serv Géol Tunisie 64:123–128

Bredehoeft JD (2002) The water budget myth revisited: why hydrogeologists model. Ground Water 40:340–345

Brunner P, Hendricks Franssen HJ, Kgotlhang L, Bauer-Gottwein P, Kinzelbach W (2007) How can remote sensing contribute in groundwater modeling? Hydrogeol J 15:5–18

Carrera J, Alcolea A, Medina A, Hidalgo J, Slooten LJ (2005) Inverse problem in hydrogeology. Hydrogeol J 13(1):206–222

Cheng AHD, Ouazar D (2003) Coastal aquifer management: monitoring, modeling, and case studies. Lewis, Boca Raton, FL

Coudrain-Ribstein A, Pratx B, Talbi A, Jusserand C (1998) Is the evaporation from phreatic aquifers in arid zones independent of the soil characteristics? CR Acad Sci Paris Earth Planet Sci 326:159–165

CRDA (2002) Rapport d'activités Commissariat Régional au Développement Agricole de Nabeul [Activity report of the Commissariat Régional au Développement Agricole de Nabeul]. Ministère de l'Agriculture et des Ressources Hydrauliques, Tunis, Tunisia

Custodio E (2002) Aquifer overexploitation: What does it mean? Hydrogeol J 10:254–277

DGRE (1985) Rapport d'exploitation des nappes phréatiques de l'année 1985 [Report of exploitation of the groundwater of the year 1985]. Direction Générale des Ressources en Eau, Ministère de l'agriculture et des ressources hydrauliques, Tunis, Tunisia

DGRE (2000) Rapport d'exploitation des nappes phréatiques de l'année 2000 [Report of exploitation of the groundwater of the year 2000]. Direction Générale des Ressources en Eau, Ministère de l'Agriculture et des Ressources Hydrauliques, Tunis, Tunisia

Diersch HG (1996) Interactive, Graphics-Based Finite Element Simulation System FEFLOW For Modeling Groundwater Flow, Contaminant Mass and Heat Transport. WASY Institute, Berlin, Germany

Doherty J (1998) PEST: model independent parameter estimation, Watermark, Brisbane, Australia

Ennabli M (1980) Etude hydrogéologique des aquifères du nord-est de la Tunisie pour une gestion intégrée des ressources en eau [Hydrogeological study of the aquifers north-east of Tunisia for an integrated management of the water resources]. PhD Thesis, Université de Nice, France

Gambolati G, Putti M, Paniconi C (1999) Three-dimensional model of coupled density-dependent flow and miscible transport in groundwater. In: Bear et al (eds) Seawater intrusion in coastal aquifers: concepts, methods, and practices. Kluwer, Dordrecht, The Netherlands, pp 315–362

Grava M (2005) Hydrochemical, hydrogeological, and geostatistical analysis of Eastern Cape Bon aquifer (northern Tunisia), Postgraduate Thesis, Centre d'hydrogéologie de l'Université de Neuchâtel, Switzerland

Hendricks Franssen JH, Brunner P, Makobo P, Kinzelbach W (2008) Equally likely inverse solutions to a groundwater flow problem including pattern information from remote sensing images. Water Resour Res 44, W0149. doi:10.1029/2007WR006097

Hichri H (2003) Annuaire hydro-pluviométrique du Cap Bon [Hydro-rainfall directory of the Cape Bon]. Ministère de l'Agriculture et des Ressources Hydrauliques, Tunis, Tunisia

INM (2001) Almanach [The climat]. Institut National de la Météorologie, Tunis, Tunisia. http://www.meteo.tn/ Cited August 2008

INS (2004) Recensement Général de la Population et de l'Habitat de 2004 [General census of population and housing 2004]. Institut National de la Statistique, Tunis, Tunisia. http://www.ins.nat.tn/. Cited August 2008

Käser D (2004) Etude hydrogéologique de la côte orientale du Cap Bon (Tunisie): apports de la télédétection à l'estimation du bilan hydrique [Hydrogeological study of the eastern coast of the Cape Bon (Tunisia): contributions of remote sensing to the estimation of water balance]. Postgraduate Thesis, Université de Neuchâtel, Switzerland

Khlaifi I (1998) Contribution à l'étude de l'intrusion marine par un modèle de transport tridimensionnel : interfaçage avec des systèmes d'information géographique [Contribution to the study

of seawater intrusion by a three-dimensional transport model: interfacing with a geographic information system]. MSc Thesis, Institut National Agronomique de Tunisie, Tunisia

Konikow LF, Kendy E (2005) Groundwater depletion: a global problem. Hydrogeol J 13:317–320

Mami A, Aloui T (1982) Carte des ressources en sols de la Tunisie: feuille de la Goulette [Map of soil resources in Tunisia: the Goulette sheet]. Directions des sols, Ministère de l'Agriculture et des Ressources Hydrauliques, Tunis, Tunisia

Milnes E, Renard P (2004) The problem of salt recycling and seawater intrusion in coastal irrigated plains: an example from the Kiti aquifer (southern Cyprus). J Hydrol 288:327–343

Nazoumou Y (2002) Impact des barrages sur la recharge des nappes en zone aride : etude par modélisation numérique sur le cas de Kairouan (Tunisie centrale) [Impact of dams on aquifers recharge in arid zone: numerical modelling study at Kairouan (Central Tunisia)]. PhD Thesis, Ecole Nationale d'Ingénieurs de Tunis, Tunisia

Oueslati A (1994) Les côtes de la Tunisie. Recherche sur leur évolution au Quaternaire [The coasts of Tunisia: research on their evolution during the Quaternary]. Imprimerie officielle de la République Tunisienne, Tunis, Tunisia

Paniconi C, Khlaifi I, Lecca G, Giacomelli A, Tarhouni J (2001) Modeling and analysis of seawater intrusion in the coastal aquifer of eastern Cap-Bon, Tunisia. Transp Porous Med 43:3–28

Parodi GN (2002) AHVRR hydrological analysis system: algorithms and theory, Version 1.3. WRES-ITC, Enschede,The Netherlands

Roerink GJ, Su Z, Menenti M (2000) S-SEBI: a simple remote sensing algorithm to estimate the surface energy balance. Phys Chem Earth, Part B Hydrol Oceans Atmos 25:147–157

Scanlon BR, Tyler SW, Wierenga PJ (1997) Hydrologic issues in arid, unsaturated systems and implications for contaminant transport. Rev Geophys 35:461–490

Steenhuis TS, Van der Molen WH (1986) The Thornthwaite-Mather procedure as a simple engineering method to predict recharge. J Hydrol 84:221–229

Tarhouni J, Jemai S, Walraevens K, Rekaya M (1996) Caractérisation de l'aquifère côtier de Korba au Cap Bon (Tunisie) [Characterization of the Korba coastal aquifer in the Cape Bon (Tunisia)]. Progress report 95–96 for AVI-73 EC Project, EC, Brussels

Winsauer WO, Shearin HM, Masson PH, Williams M (1952) Resistivity of brine-saturated sands in relation to pore geometry. AAPG Bull 36:253–277

 DOI 10.1007/s10040-010-0573-5